SUPPLEMENTARY MATERIAL

The numerical model. To investigate mechanisms, it is sometimes most productive to run a large number of simplified simulations rather than a limited number of detailed simulations. The numerical tests reported here are based upon the *FLAC* continuum code with distributed ubiquitous joint zones to represent the natural fractures. An inherent assumption is that fractures (including faults) can slip but not propagate. In a layered, densely fractured medium, propagation will in many instances be resisted by intersection with other fractures (e.g. Zhang *et al*. 2006) and weak bedding planes such as encountered in the Bowland Shale (Harper 2011). To some extent, this mitigates the absence of a fracture propagation option, which would make the code far more cumbersome. The code does, however, allow the spontaneous growth of new faults as narrow shear zones in the Mohr-Coulomb continuum (Cundall 1990). Clark (2011) showed that pre-existing faults can be simulated using a series of adjacent ubiquitous joint zones.

FLAC (Itasca 2011) is an explicit finite difference computational mechanics code which has been commercially available for more than thirty years and has been widely used and tested. A range of constitutive models, including the ubiquitous joint model implemented here to represent fractures, are available as standard options. The ubiquitous joint option represents a linear Mohr-Coulomb material with planes of weakness of specified strength and orientation described by Jaeger and Cook (1971). In FLAC, groups of natural fractures with variations of properties and orientations specified by a standard deviation can be specified. Zones devoid of natural fractures were allocated Mohr-Coulomb constitutive properties (elastoplastic). Additional code can be added in *FLAC* by the user which makes the code extremely adaptable. Uses of this option included the distribution of the natural fractures and their properties randomly throughout the grid, monitoring of slip increments on natural fractures and imposition of a pore pressure distribution representative of a stimulation treatment.

Effective stress computations were conducted without groundwater flow but with a change of total stress automatically implemented (assuming Biot's constant = 1) when a fluid pressure change is imposed by the user. In this mode, *FLAC* correctly represents the reservoir deformations induced by imposed pore pressure changes during stimulation. *FLAC* v7 has inbuilt double precision so that the changes of stress and displacement associated with geomechanical changes such as slip on fractures and pore pressure changes (including seepage forces induced by pore pressure gradients) are accurately represented even in large models. Two-dimensional 5 x 5 km plan view models (plane strain) of the simulated shale reservoirs were constructed with 10 m x 10 m zones . First, the stress states (including a uniform reservoir pore pressure) were initialised in and at the boundaries of Mohr-Coulomb continua with the required intact material properties. This includes the out-of-plane stress corresponding to a depth of 3000 metres, assuming a gradient of the vertical stress of 22.62 MPa/km (1 psi/ft). Variations of elastic moduli can be readily implemented. Although a marked variation of elastic moduli is typical some if not most shale reservoirs, this option was omitted to simplify interpretation of the simulation results.

Preparation of the reservoir models. Once the stress-controlled Mohr-Coulomb models had equilibriated, the boundary conditions were changed to roller boundaries (no displacement perpendicular to the boundary but displacements permitted parallel to the boundary without any restraint). The reservoirs with displacement-controlled boundary conditions were again cycled to equilibrium before introducing the populations of natural fractures (with or without a fault), all fractures being assumed to be vertical. A third period of equilibriation followed. As noted, in the examples presented here, no-displacement roller boundaries were imposed (displacement control). Other reservoirs have been tested retaining stress-controlled boundaries for comparison and these tended to have moderately less variation in the stress state. The characteristic behaviour when subject to stimulation was similar for either stress-controlled boundaries or displacement-controlled boundaries.

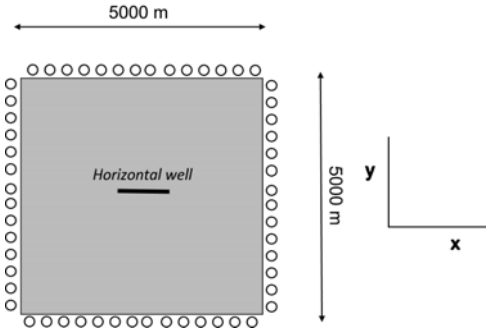

Supplementary Fig. 1. Schematic layout of the numerical simulations after changing from stress-controlled boundaries to displacement control. Plan view illustrating model geometry (5000 m x 5000 m, roller boundaries, 250000 square finite difference zones, Mohr-Coulomb continuum with 30% or 40% ubiquitous joint zones simulating natural fractures) and central horizontal well from which 10 vertical hydraulic fractures are simulated successively and spaced at 100m. In the initial condition, prior to natural fracture emplacement, the maximum normal stress was applied parallel to the y-axis, the minimum normal stress parallel to the x-axis and the out-of-plane stress corresponding to the depth of burial applied normal to the diagram. The model was allowed to reach equilibrium before changing to the displacement-controlled boundaries illustrated.

A large number of cycles were allowed in equilibriating the fractured reservoir, monitoring the slip events (slip increments) as the reservoirs approached equilibrium. Each recorded increment of slip depends upon the solution timestep. As the timestep was found to vary by only a minor amount, these increments provide a good approximation of the spatial distribution of slip magnitude within the fracture network. A significant proportion of the fractures experienced slip as the reservoir approached equilibrium, the slip only ceasing at the point where the resisting forces balanced the disturbing forces associated with the local stress field. Once equilibriated, the result in each case was a fractured reservoir in a state of marginal equilibrium. Despite the very large number of cycles allowed (10^6), occasionally a slip increment on a natural fracture somewhere in the 5 x 5km reservoir could still be detected. This was interpreted as long-range interaction (see main text) influenced by work done at the boundaries to maintain the displacement control condition.

Hydraulic fracture stimulation. Multistage stimulation in the central portion of each reservoir was simulated simply by sequential phases of imposed pore pressure increase at locations separated by 100m. Each hydraulic fracture stimulation was simulated by the simple expedient of instantly imposing an identical, approximately elliptical pore pressure distribution at each stage location. (Each stage was assumed to have a single set of perforations.) A simple trial of a two-stage pressure rise showed no significant difference in the results. The magnitude of the maximum pressure at the injector location was chosen to be larger than the minimum applied total stress and smaller than the applied vertical total stress. Reservoir A was fracture treated with a net pressure of 11.4 MPa (approximately 2000 psi) and reservoir B at a net pressure of 3.3 MPa (approximately 500 psi). The imposed pressure distribution corresponded approximately to a steady-state flow condition [the approximation arising from interpolation across a finite zone size (10 m x 10 m)]. In the cases presented here, the treatment stages were identical. The mechanical response of the reservoir in the vicinity of the stimulation stage and elsewhere can be observed and typically included mode 1 (extension) failure near the well and slip on suitably orientated pre-existing natural fractures (ubiquitous joint zones).

As stated previously, no flow was allowed, the pore pressure distribution was held constant for a time sufficient for some degree of equilibriation to occur. (The durations of the injection periods and intervals between fracture treatments in real situations are finite and achievement of an equilibrium state between each treatment can not be assumed.) Any chosen pressure distribution can be implemented so that comparisons of the effect of different elliptical pressure distributions can readily be made. Although sequential imposition of identical elliptical pressure distributions is a gross simplification of the fracturing process, it greatly speeds the calculation process and, importantly, simplifies the interpretation of reservoir response. [Readers are also reminded that reliable, precise

prediction of fracture growth is inherently unpredictable for several reasons; first, the process of fracture propagation in fractured media is highly nonlinear (mainly because the flow of fluid is threshold (frictional limit) -dominated and flow rate is a power of fracture aperture: see Harper and Last 1990); second; the details of fracture distribution and mechanical properties remote from the well are unknown].

Ten sequential stages were simulated. A single stimulation treatment might have sufficed to indicate the stress memory effect. However, at the spacing of 100 m simulated here (currently typical of the spacing employed in many horizontal shale wells), considerable interference between fractures can occur and the resulting elongate stress concentration is likely to be more typical of real situations (almost always sequential fracture treatments exceeding 10 in number are carried out by a shale gas operators.) Moreover, the mechanical response of each region of pore pressure rise (simulated fracture treatment) is different. Restricting the simulations to single treatments would not only be unrepresentative of operational practice but would also risk uncertain conclusions.

Each slip increment (as equilibrium was approached) on all natural fractures throughout the reservoir was counted and mapped in space as a guide to the evolution and distribution of slip on all the natural fractures during the fracture stimulation sequence. The number and distribution of slip events (slip increments) on natural fractures and the fault during the multistage fracture stimulation can be taken as a comparative guide to the potential for, and distribution of, induced seismicity because the time steps did not differ significantly between the different simulations for each reservoir. (This assumes none of the slip increments are aseismic.) Contours of the number of slip increments are used in Figures 6 of the main text to indicate the distribution of slip. Supplementary Fig. 2 is a magnified example to illustrate the contouring in more detail.

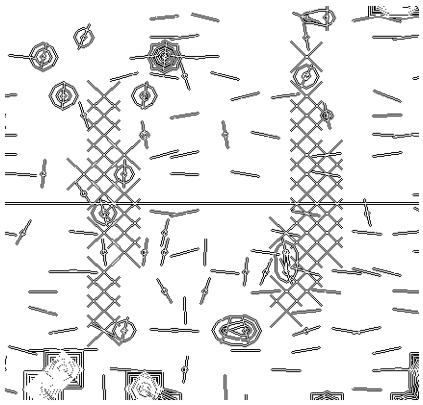

Supplementary Fig. 2. 200m x 200m plan view of part of Reservoir A showing detail of the contours of slip increments (slip events) induced on natural fractures by the elliptical zones of pore pressure rise representing two fracture treatments. The post-stimulation stage is represented so that the imposed elliptical pore pressure distributions, equivalent to steady state flow in an isotropic medium, are not shown. The horizontal straight line crossing the figure denotes the hypothetical horizontal well. Individual short lines, approximately 10m in length, represent natural fractures. A dot in the centre of a natural fracture denotes past slip induced either as the reservoir approached equilibrium or during the stimulation treatments. Crosses mark 10x10m zones in which failure of intact rock, in shear or tension, occurred during stimulation. Contours of slip increments in individual ubiquitous joint zones change from rounded to square (the zone shape) as the number of increments increases.

The two shale reservoir formations. No stress data were given by Sorensen *et al*. (2010) for the Barnett Shale reservoir. Partly guided by the values used by Palmer *et al*. (2007) to model the Barnett Shale, the gradient of the maximum horizontal stress was assumed to be 20.34 MPa/km (0.9 psi/ft),

the gradient of the minimum horizontal stress assumed to be 13.57 MPa/km (0.6psi/ft) and the pore pressure gradient assumed to be 11.76 MPa/km (0.52 psi/ft). (All gradients refer to reservoir depth.)

For the reservoir in a strike slip environment, a combination of extension fractures subparallel to the maximum horizontal stress and shear fractures subparallel to the planes of maximum shearing stress and a pore pressure gradient of 11.31 MPa/km (0.5 psi/ft) were assumed. The gradient of the maximum horizontal stress input to the model was 28.275 MPa/km (1.2 psi/ft) and the input minimum horizontal stress gradient was 16.97 MPa/km (0.75 psi/ft).

Both reservoirs were assumed to be 3000m deep and subject to an overburden stress gradient of 22.62MPa/km (1psi/ft). Each model has a central fault of 170m length inclined at 45^0 to the maximum applied horizontal stress with identical frictional and cohesive properties to the natural fractures. Table 1 summarises the main input parameters for the two models.

Reservoir	Faulting environment	Modulus		Friction angle	SD	cohesion	SD	tensile strength
		Bulk Pa	Shear Pa	deg.		Pa		Pa
A	normal	1.58e10	7.3e9	40	2	3.4e7	3e2	3e6
B	strike slip	1.25e10	5e9	27.5	1	1e7	1e2	1e6

Table 1a. Properties assumed for the intact shale. SD denotes standard deviation.

Reservoir	total %	%	median azimuth deg.	SD	%	median azimuth deg.	SD	%	median azimuth deg.	SD	friction angle deg.	SD	dilation angle deg.	tensile strength Pa
A	30	20	90	10	10	0	15				20	1	5	5e5
B	40	20	0	10	10	45	10	10	315	10	15	0.5	5	1e5

Table 1b. *Properties assumed for fractures.* Azimuths are clockwise from North.

References

Clark, I.H., 2011. Simulation of rock mass strength using ubiquitous joints in 3D. *In*: Sainsbury, D., Hart, R.D., Detournay, C.L. & Cundall, P.A. (eds) *Continuum and Distinct Element Numerical Modeling in Geo-Engineering – 2008*, Proceedings of the 1st International *FLAC/DEM* Symposium, 25-27 August 2008, Minneapolis. Itasca Consulting Group, Inc.

Cundall, P.A., 1990. Numerical modelling of jointed and faulted rock. *In*: Rossmanith, H.P. (ed) *Mechanics of jointed and faulted rock*: Proceedings of 3rd International Conference on Jointed and Faulted Rock, Vienna, 6-9 April, Taylor & Francis.

Itasca 2011. FLAC Users Guide v7.0, Itasca Consulting Group, Minneapolis.

Jaeger, J.C. & Cook, N.G.W. 1971. *Fundamentals of rock mechanics*, Chapman & Hall.

Palmer, I., Moschovidis, Z. & Cameron, J. 2007. Modeling shear failure and stimulation of the Barnett Shale after hydraulic fracturing, *Society of Petroleum Engineers*, SPE 106113.

Thompson, J.M.T. & Stewart, H.B. 1986. *Nonlinear dynamics and chaos*, John Wiley and Sons, Chichester.

Zhang, X., Jeffrey, R.G. & Thiercelin, M. 2006. Deflection and propagation of fluid-driven fractures at frictional bedding interfaces: A numerical investigation, *Journal of Structural Geology*, 29, 396-410.